Uncertainty in wave basin testing of a fixed oscillating water column wave energy converter

Authors: Frances Judge[1*]; Eoin Lyden[1]; Michael O'Shea[1]; Brian Flannery[1]; Jimmy Murphy[1]

Affiliations: [1] MaREI Centre, Environmental Research Institute, University College Cork

* Correspondence to frances.judge@ucc.ie

Abstract

This research presents a methodology for carrying out uncertainty analysis on measurements made during wave basin testing of an oscillating water column wave energy converter. Values are determined for Type A and Type B uncertainty for each parameter of interest, and uncertainty is propagated using the Monte Carlo method to obtain an overall Expanded Uncertainty with a 95 % confidence level associated with the Capture Width Ratio of the device. An investigation into the impact of reflections on the experimental results reveals the importance of identifying the incident and combined wave field at each measurement location used to determine device performance, in order to avoid misleading results.

1 Introduction

Laboratory testing is critical for the development of viable wave energy converters (WECs) as the use of physical scale models provides the opportunity to prove and validate a concept at relatively low cost. This enables the progression of technology through the low Technology Readiness Levels (TRLs) and on to open water testing. The European Commission has defined a TRL scale for technology development [1] and laboratory testing fits into TRL3 (Experimental proof of concept) and TRL4 (Technology validated in laboratory). Specifically for WEC development, the detail of TRL 3 and 4 have been more precisely defined in terms of the complexity and scale of the testing that should be undertaken: i.e. the type and size of test facility that is required, the range of test conditions, the degree of instrumentation and measurement, the model scale used and the representation of the power take-off (PTO) system.

For WEC development, perfect chronological continuity and comparability of results as the device concept evolves to higher TRLs is difficult to achieve. However, an understanding of how metrics such as power performance differ between various tank testing campaigns is required to make informed decisions as the concept develops. As yet there is not a quantitative understanding of the variance in results from different tanks testing campaigns where the same WEC technology has been tested in different test tanks or at different scales. An important element of this comparison is understanding the uncertainty associated with different tanks/flumes and how this uncertainty is reflected in device performance metrics.

Tank testing of WECs and other offshore renewable energy (ORE) devices involves measurement of different parameters from which device performance and feasibility can be assessed. Each measurement is accompanied by an associated uncertainty and therefore can only provide an estimate of the 'true' value of that parameter. Uncertainty analysis can provide a lower and upper limit, between which the true value of a measurement lies and therefore gives an indication of the quality of the measurements made.

In terms of previous related work, Qiu et al. [2] discuss the parameters that introduce uncertainty into physical testing at model scale and divide them into the following categories: fluid properties, initial test conditions, model definition, environment, instrumentation, scaling and human factors. Robertson [3] applies the American Society of Mechanical Engineers method [4] for assessment of uncertainty in tank testing of semi-submersible offshore wind models. Desmond et al. [5] investigate the trade-off between accuracy and precision in tank testing of a floating offshore wind platform. The types of uncertainties encountered during tank testing of a floating offshore wind model are similar to those associated with WEC model testing.

Uncertainty analysis studies focused specifically WECs are sparse. Preliminary work on the EquiMar project [6] sets out a procedure for assessing physical tank testing uncertainty related to scale wave energy devices. Expanding on this, Orphin et al. [7,8] presents the first fully developed uncertainty analysis of physical tests of a fixed OWC at the Australian Maritime College (AMC). The present work applies similar analysis techniques to quantify the sources of uncertainty encountered during a wave energy tank testing programme at the Lir National Ocean Test Facility (Lir NOTF) in University College Cork.

1.1 Aim of this research

The aim of this research paper is to identify the sources of uncertainty associated with laboratory testing of a fixed Oscillating Water Column (OWC) WEC; calculate the uncertainty associated with the measurements made (measurement uncertainty) and propagate the uncertainty to obtain an overall assessment of the uncertainty of the capture width ratio of the device; and provide a methodology for performing uncertainty analysis that others may follow. This research also aims to examine the impact of reflections on experimental results, and make recommendations as to how overall uncertainty can be reduced to increase confidence in results.

2 Sources of uncertainty in tank testing

The sources of uncertainty encountered during tank testing of scale WECs can be categorised as follows: measurement uncertainty, model uncertainty and environmental uncertainty. The types of uncertainty in each of these categories can be described in several ways: Random and Systematic, Type A, Type B etc. These are discussed in more detail in Section 3 of this paper.

2.1 Measurement Uncertainty

All measurements have an element of uncertainty, and a description of that uncertainty should be given (i.e. as a ± range associated with the measurement) to indicate the accuracy of the measurement. In tank testing there are usually multiple measurement modes of various parameters using a range of instruments. The measurement uncertainty therefore is related to the accuracy of the instruments used. These instruments range from water level gauges, pressure sensors, load cells, strain gauges as well as advanced motion capture and laser recording systems, each with an associated accuracy which should be factored into the uncertainty analysis. To mitigate against uncertainties in sensor measurement such as hysteresis, drift etc., it is good practice to undertake regular instrument calibration. Instrument setup inconsistencies can also contribute to measurement uncertainty; loose fittings, wiring and unstable mounting of instrumentation are potential sources of error. Measurement uncertainty can also be influenced by the conditions in the test facility such as ambient temperature, humidity and tank water turbidity. While good housekeeping protocols in tank facilities should eliminate such sources of uncertainty, it can become an issue when comparing results across facilities in different climates.

In the current study, the instrumentation used are wave gauges and pressure sensors. The layout and orientation of these instruments are discussed in Section 4. A wave gauge comprises two parallel metal rods partially immersed in the water. The change in resistance of the rods as the water level changes is converted to water elevation (mmH20) and typically an error of 0.1% can be achieved [10]. Regular calibration and accurate installation of these gauges is required to achieve such low levels of associated error. Pressure sensors are generally piezoresistive, and measure pressure based on the change of electrical resistance of a material in response to change of pressure. The error in pressure measurements (typical contribution to the total error shown as a percentage) can be due to nonlinearity hysteresis (~0.5%) thermal sensitivity (~3% over -18deg c to +93deg c range), and pressure directional sensitivity (~1.5%+-0.5).

2.2 Model Uncertainty

There is an inherent uncertainty introduced by reducing a full-scale prototype to a simplified scaled model to undertake performance analysis in the controlled environment of a laboratory. In a tank testing scenario, one or more of the following effects are generally ignored: viscosity, surface tension, stiffness and/or compressibility. These simplifications limit the accuracy to which the scale model can represent the prototype being tested. Scaling laws such as Froude scaling and Reynolds scaling [9,10] are typical methods to mitigate this uncertainty. Such laws have their limitations however and cannot capture all physical quantities, e.g. air compressibility, which is often ignored at small scale (i.e. incompressibility is assumed). This can be significant when considering OWCs at full scale which use water oscillation driven pressurisation of air in the chamber to drive a turbine. The effect of air compressibility can be simulated in a scaled model by utilising deformable chambers [11], or a series of reservoirs [12]. However, at smaller model scales (1:30 – 1:50) incompressibility is often assumed. Assuming isentropic air flow (adiabatic and reversible) has been shown as a valid approach to accounting for compressibility at model scale testing of OWCs by [13]. The performance impact of these assumptions was dealt with by [14] whereby a compression number was developed to show relative importance of compressibility in OWCs. For the scale model example in [14] which is similar to the OWC in the current study, the compression numbers calculated over a series of different test conditions indicated compressibility effects were negligible.

The orifice in an OWC is where the critical performance metrics are measured. At this location the flowrate of air forced through the constriction is used to drive the PTO. Flow rates are often calculated using the discharge coefficient associated with the orifice plate used to replicate the PTO during testing. The calibration of these plates involves curve fitting of a series of results which introduces uncertainty. The calibration process can be undertaken in a number of ways, from manually displacing the device and taking measurements or else mechanical excitation, that is to drive the device with a motor and guide rail setup. Using a motor for forced oscillations allows for more controlled (in comparison to manual excitation) sinusoidal as well as ramp type measurements to be taken. The representation of the PTO by an orifice is a simplification that represents a significant source of uncertainty. Other sources include hydrodynamic loads and the incident wave climate. [8] attempted to quantify scale effects by studying the performance of an OWC at three different scales (1:20, 1:30 and 1:40) and found large differences in the power performance of the three models. These differences were primarily attributed to the PTO damping and variations in the incident wave conditions due to the variations in the placement of each model in the basin. The study concluded that while further investigation is required, scale effects may account for uncertainties of the order $\pm$15%.

Model discrepancies, apart from idealisation and simplification, include fabrication accuracy, buoyancy and density. These issues are more critical in floating models; for fixed models such as fixed OWCs, geometric discrepancies can be accounted for by repeat measurements of the critical areas such as internal geometry and orifice diameter.

2.3 Environmental uncertainty

The most complex source of uncertainty relates to the testing environment produced in the wave basin. The uncertainty related to wave height, period and direction generated in the basin has several sources which contribute to reduction in accuracy of the testing process. The physical attributes in the tank including wave generation system, depth, tank walls and dissipative beach result in a non-uniform distribution of wave statistics for any given input condition. These sources of uncertainty can be reduced by undertaking a wave calibration exercise prior to the planned test campaign. This involves varying the wave maker input values to achieve the required incident conditions at the location of interest in the tank (model location). A typical test campaign will run the test plan without the scale model in place as a control.

The influence of reflections within basins has a significant influence on the temporal variation in wave statistics. This is compounded by the fact that the effect of reflections varies with wave parameters (T_s, T_p). The interaction of reflected and incident waves can distort power performance calculations of the device being tested either positively or negatively. There are several methods to reduce this source of uncertainty including during set up and raw data analysis as well as at the post processing stage. During regular wave test runs, there can be a clear delineation in the recorded time series of water elevations between the clean incident wave and when reflections begin to influence the data collection. This section of the recorded time series can be used in analysis, however as the delineation point will vary with respect to wave period due to celerity of the incident and reflected wave, automation of this analysis methodology can be difficult and become impractical for large test programmes. The approach is also only valid for that location in the wave tank. An alternative approach which is valid for both regular and irregular waves is applied in the post processing phase but requires additional wave gauges to measure reflection. The raw data series is separated out into incident and reflected wave statistics. Funke and Mansard [15] improved the initial approach of Goda and Suzuki [16] using Fourier analysis. This relies on recording a series of water elevations at distinct intervals related to the wavelength of the incident wave to extract reflection statistics. The influence of reflections in the present study is presented in Section 6. Even with applying these techniques there are uncertainties not accounted for including the wave spreading limitation and low frequency excitations which cannot practically be mitigated against.

The values of parameters used in post-processing calculations such as the water density in the test facility and the acceleration due to gravity have associated uncertainties which should be accounted for in any assessment of uncertainty and are discussed further in Section 5.

3 Uncertainty analysis

There are several nomenclatures for describing uncertainty and measurement error, i.e. the difference between a measurement and the true value of a quantity. Bias refers to systematic or non-random errors; it describes the difference between the average of all measurements made of the same quantity and the true/reference value. Precision on the other hand describes how close all measurements are to each other and is thus an indication of the repeatability of the measurements. Bias and precision errors can also be referred to as systematic and random errors. This is the classification adopted by the American Society of Mechanical Engineers and is used in the uncertainty studies undertaken by [3,5].

In this research, the ISO-GUM methodology [17] is followed, which is also described in the International Towing Tank Conference guideline ITTC 7.5-02-07-03.12 [18]. This method categorises uncertainty under the following three headings: standard uncertainty (u_s), combined uncertainty (u_c), and expanded uncertainty (U).

Standard uncertainty can be further described as Type A or Type B. Type A uncertainty (u_A) is obtained by applying statistical methods to repeated measurements and is calculated from

$$u_A = \frac{s}{\sqrt{n}}, \qquad (1)$$

where n is the number of repeat measurements and s is the standard deviation, given by

$$s = \sqrt{\frac{\sum_{k=1}^{n}(q_k - \bar{q})^2}{n-1}}, \qquad (2)$$

in which q_k is the k^{th} observation and $\bar{q}$ is the mean. It therefore represents precision or random errors.

Type B uncertainty (u_B) is usually evaluated using means other than repeated tests such as manufacturers' specifications, calibration data and scientific judgement. It can be calculated by applying a linear fit to the end-to-end calibration data of the relevant instruments (i.e. wave probes and pressure sensors). u_B is then given by the Standard Error of the Estimate (*SEE*):

$$u_B = SEE = \sqrt{\frac{\sum(y_j - \hat{y}_j)^2}{M-2}}, \qquad (3)$$

where $M = j_{max}$ is the number of calibration points, y_j is the data point and $\hat{y}_j$ is the fitted value. In this research, M varied from 6 points for wave probe calibration, to 21 points for pressure sensor calibration.

Type A and Type B uncertainty can then be combined as follows to give the standard uncertainty of a measurement:

$$u_s = \sqrt{u_A^2 + u^2}_B. \qquad (4)$$

The end-result of a laboratory test is often calculated from several measurements rather than measured directly. Therefore, the uncertainties associated with each measurement must be combined appropriately in order to calculate the uncertainty in the final result. This can be done in a number of ways. The ITTC guidelines [18] describe the law of propagation of uncertainty, which involves formulating a Data Reduction Equation (DRE) using a first-order Taylor expansion that combines the standard uncertainty of each relevant quantity (Equation (4) in [18]) However, the DRE can be challenging to formulate and statistical methods of propagating uncertainty are a practical alternative. In this research, the Monte Carlo method is implemented, following the research of [19]. Monte Carlo methods are computational algorithms that have widespread applications across the engineering spectrum. In the renewable energy sector, Monte Carlo methods have been to evaluate the uncertainty in results produced using deterministic processes from lifecycle analysis for example [20] to structural design [21].

Briefly, the Monte Carlo (MC) method involves running N independent iterations of a model (e.g. calculating the power produced by an OWC) where each iteration involves random sampling of values from a probability distribution that characterises each stochastic variable. In this research, the stochastic variables include the wave height and pressure (for a full list see Table 3). Standard uncertainties are calculated where possible for each variable and are assumed to represent the standard deviations of a Gaussian probability distribution function. Each MC iteration then takes a random sample of the probability distribution function of each quantity to calculate the result. The uncertainty associated with the final result is then evaluated from the standard deviation of all the Monte Carlo iterations.

Once the combined uncertainty, u_c , has been determined, the expanded uncertainty, U, can be calculated. This is simply a statement of the overall uncertainty at a particular confidence level, typically 95%, and is given by

$$U = ku_c , \qquad (5)$$

where k is a coverage factor whose value is dependent on the number of samples/repeats and the confidence level required and can be read from *t*-distribution tables.

4 Experimental setup

The device being tested is a 1:30 scale fixed nearshore bent-duct OWC with a low Technological Readiness Level (TRL), constructed out of perspex and fitted with wave probes, pressure sensors and a 15 mm diameter orifice. A fixed wave energy converter was chosen for this research as it eliminates any uncertainties linked to the motion of the device and therefore provides a more straightforward template for uncertainty analysis. Fixed OWCs are typically designed for integration into breakwaters at coastal locations. The present model was designed by Ecole Centrale de Nantes for use in the MaRINET2 project[1] A similar device has been tested at the Australian Maritime College to carry out an uncertainty analysis of an OWC [7].

The device was tested in the Ocean Basin (OB) at the Lir NOTF in UCC (Figure 1). The OB is a 25m x 15m wave basin with an adjustable floor to facilitate testing at water depths between 1m and 2.5m. The wavemaker consists of a curved bank of 80 hinged paddles which forms two sides of the basin and allow a wave direction range of more than 100 degrees. The paddles are equipped with active absorption; this feature coupled with an absorbing beach structure on the other two sides of the basin improves wave conditions and settling times between tests.

Figure 1 Ocean basin at the Lir NOTF, Cork

[1] www.marinet2.eu

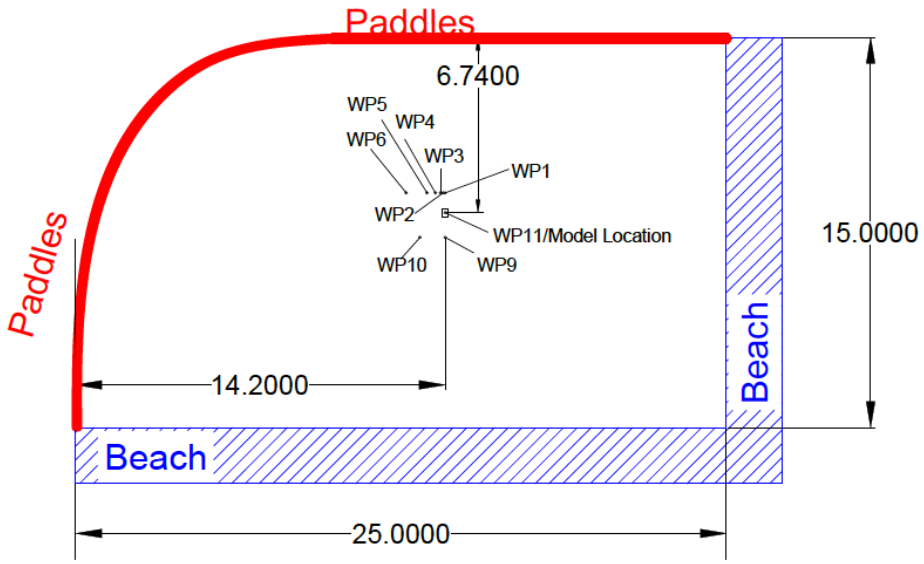

Figure 2 Model location within Lir NOTF Ocean Basin

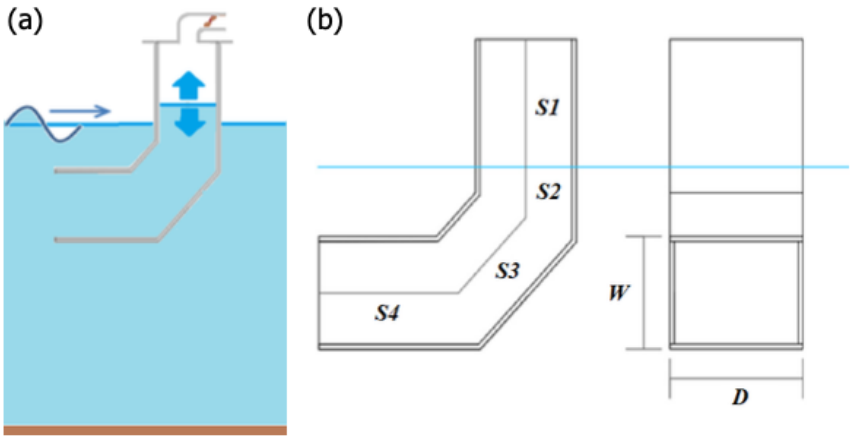

Dimensions [m]	1 :30	Full scale
D (external)	0.300	9
W (external)	0.236	7.08
Wall thick.	0.008	0.24
S_1	0.260	7.8
S_2	0.103	3.09
S_3	0.217	6.51
S_4	0.318	9.54
depth	1.000	30

Figure 3 OWC schematic and dimensions

The location of the model within the Ocean Basin is shown in Figure 2. A schematic of the model and the key dimensions are presented in Figure 3. Testing was conducted at a water depth of 1m. A wave probe was set up at the model location for the purposes of wave calibration and a line of additional probes were installed adjacent to the model to enable an analysis of the reflections in the basin (see Figure 2). During the model installation, the incident wave probe was removed and replaced with the OWC in which 3 wave probes and 2 pressure sensors were mounted within the chamber (see Figure 4)

Meggit 8510b-2 pressure sensors were used to measure the oscillating pressure inside the chamber with a sampling rate of 32 Hz; these are piezoresistive pressure transducers that measure relative pressure. The pressure sensors were chosen for their robustness, small size and accurate dynamic response. The instrument accuracy is a contributor to overall systematic uncertainty, while setup of the instruments can contribute to random uncertainty.

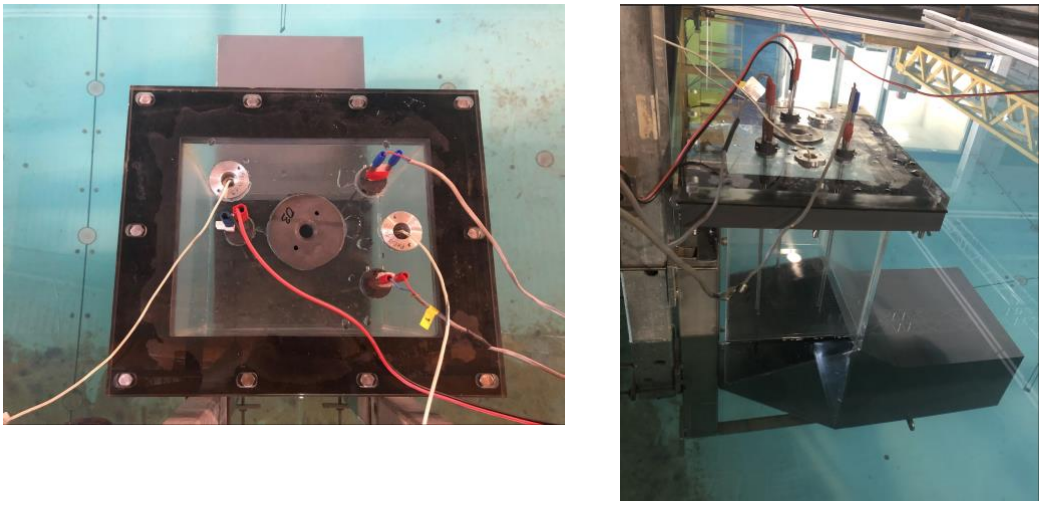

Figure 4 Wave probe and sensor layout within the OWC

5 Uncertainty evaluation

5.1 Standard uncertainty evaluation

5.1.1 Type A

Type A uncertainty is evaluated for a sample of both regular and irregular waves with a view to calculating the uncertainty of the capture width ratio (CWR),

$$CWR = \frac{P_{owc}}{P_{inc}D} \quad , (6)$$

where P_{owc} is the power generated by the OWC, P_{inc} is the power of the incident waves, and D is the width of the OWC. Calculating an uncertainty range for the CWR necessitates a set of repeat tests on the incident wave field at the model location (i.e. without model in place) and a second set of repeats with the model in position.

For the regular waves, repeats were carried out at the wave height (H = 0.025 m) and period (T = 1.64 s) that indicated the best device response (identified from preliminary tests) and at periods towards the lower (T = 1.26 s) and higher (T = 2.19 s) end of the range (T = 0.73 s to 2.56 s) using the same wave height. ITTC guidance on uncertainty analysis [18] advises that a minimum of n = 10 repeats is necessary to determine the probability distribution function from which the statistics of interest can be calculated. In this research, the method of [7] is followed whereby individual waves in each regular wave run are considered to represent 1 of n. The individual waves were chosen by examining each recorded time series, excluding transient waves and selecting waves with a consistent wave height early in the time series before reflected waves reach the device location. Using this method, the number of 'clean' waves from each wave run varied between 5 and 10 depending on the period, with longer periods resulting in fewer clean waves.

The Type A uncertainty associated with the wave height ($u_{A-\eta,inc}$) and the period, ($u_{A-T,inc}$), was then calculated for each of the incident waves in Table 1 using Equation 1. A similar procedure was then

applied with the OWC installed in the basin to obtain the Type A uncertainty associated with the water level ($u_{A-\eta,owc}$) and pressure ($u_{A-Pr,owc}$) **)** in the OWC chamber. The values are presented in Table 1.

Table 1 Repeated regular waves and associated Type A values

Input *H* (m)	Input *T* (s)	*n*	Measured *H* (m)	Measured *T* (s)	$u_{A-\eta,inc}$	$u_{A-T,inc}$	$u_{A-\eta,owc}$	$u_{A-Pr,owc}$
0.025	1.26	50	0.02466	1.2792	0.443 %	0.120 %	0.360 %	0.531%
0.025	1.64	40	0.02778	1.6364	0.751 %	0.184 %	0.280 %	0.452 %
0.025	2.19	25	0.02669	2.1770	1.052 %	0.233 %	0.468 %	0.997 %

The repeat tests carried out on the irregular waves were also chosen based on the resonant period; i.e. the peak wave period (T_p) in the test plan closest to 1.64 s. Three different significant wave heights (H_s) were selected at this period to ensure a good dynamic response (see Table 2) and 5 repeats were carried out for each sea state with incident waves only, and with the OWC installed in the basin. Irregular waves were generated using a Jonswap spectrum with a peak enhancement factor γ = 3.3, and a repeat period of 11 minutes. The resulting time series contained approximately 473 individual waves. The method for assessing Type A uncertainty for irregular waves is slightly different to the regular method, as it is not possible to extract individual waves to increase the sample size. Instead, the incident wave power was calculated directly for each repeat using Equation 10 and the Type A uncertainty determined from the results using *n* = 5 (presented in Table 2).

Table 2 Repeated irregular waves and associated Type A values

Wave type	H_s (m)	T_p (s)	No. of repeats (*n*)	$u_{A-Pw,inc}$
Irregular	0.025	1.72	5	0.37 %
Irregular	0.042	1.72	5	0.39 %
Irregular	0.058	1.72	5	0.42 %

general, the Type A uncertainty values are low, indicating a high level of precision/repeatability across the tests. The highest uncertainty for all metrics is observed in the *T* = 2.19 s regular waves, indicating less accuracy for longer periods due to the smaller number of samples in the dataset.

5.1.2 Type B

Type B uncertainty was evaluated from the calibration data for the instruments used to take measurements, i.e. the wave probes and pressure sensors and well as from the documented instrument sensitivities. Wave probe calibration was carried out by fixing the probes onto a calibration frame that allows the probes to be moved up and down by 50 mm intervals. Six calibration points were used, including the start and finish (zero) position (a 200 mm range). By varying the immersion depth by a known distance, a relationship is established between the immersion depth and the voltage response to which a linear fit is applied. The Type B uncertainty value is then given by the standard error of the estimate (Equation 3).

Where a probe was calibrated in a different location to where it was used during testing (i.e. the probes within the OWC chamber), the probe was zeroed when moved to its final location after calibration. The present model has three wave probes measuring the free surface elevation of the

water column; each probe was calibrated using the procedure outlined above, and the average Type B uncertainty is presented in Table 3 (η_{owc}).

The pressure sensors were calibrated using an Additel 760 pressure calibrator which automatically generates specified pressures with high accuracy using an in-built electronic pump. An example of the resulting calibration data is presented in Figure 5. The Type B uncertainty (i.e. the SEE) was calculated in the same manner as for the wave probes using Equation 3, but with 21 calibration points, ranging between -20 and 20 mbar, where the fitted values have been converted from V to mbar using the slope of the line.

The Type B uncertainties due to both instrument calibration and sensitivity are listed in Table 3 and denoted by 'calib' and 'sens' respectively. An uncertainty of 0.1% has been assumed for the instrument wave probe sensitivity and a value of 1.5% for the pressure sensors based on the instrument data sheets. In the case of the pressure sensors, this value includes errors due to nonlinearity, pressure hysteresis etc. as discussed in Section 2.

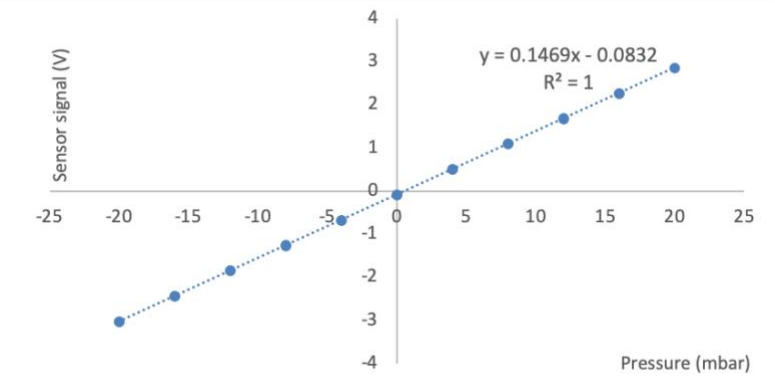

Figure 5 Pressure sensor calibration data: calibration points and linear best fit

The standard uncertainty of each variable is calculated according to Equation 4 and the results are presented in Table 3. Where more than one Type B uncertainty was associated with a variable, e.g. η, the standard uncertainty was calculated from $u_s = \sqrt{u_A^2 + u_{B1}^2 + u_{B2}^2 + \cdots}$. Included at the bottom of Table 3 for reference are the standard uncertainties for the acceleration due to gravity, g, and the density of water, ρ_w. The former value was obtained from [18] whereas the latter was estimated using ITTC 7.5-02-01-03 (Fresh Water and Seawater Properties) [22] and accounts for temperature variation in a tank hall setting. The uncertainty associated with the water depth, which accounts for unevenness in the floor, was based on spot measurements taken by hand with a 2 m long staff during the testing process. This value includes a least count error estimate for the measurement based on professional judgement. Least count errors for the data acquisition used in the experiments were found to be 5.0 x 10^{-11} m for the wave probes and 5.0 x 10^{-9} Pa for the pressure sensors, and therefore were considered negligible and not included in the analysis.

A standard uncertainty of Z = 2 % is assumed to account for uncertainties due to non-measured factors such as air compressibility and wave nonlinearities that may impact the results. It should be noted that the purpose of this figure is to account for uncertainties that effect a model of this scale, and is not an attempt to quantify the uncertainty due to scale effects (see discussion in Section 2.2). The latter would require a detailed investigation beyond the scope of this study; the focus of this research is on quantifying measurement uncertainty. The figure of Z = 2 % has been assumed based on engineering judgement; however, a sensitivity study has been undertaken using values of Z between 0.5 % and 10 % to determine the impact on the overall expanded uncertainty (see Section 5.1.5).

345 *Table 3 Type A, Type B and standard uncertainty for parameters of interest*

		Parameter	Mean	u_A	u_B	u_s
Regular waves	H=0.025 m T=1.24 s	η_{inc}	0.0247	0.443 %	0.130 % (calib.) 0.100 % (sens.)	0.472 %
		T_{inc}	1.279 s	0.120 %	-	0.120 %
		η_{owc}		0.360 %	0.167 % (calib.) 0.100 % (sens.)	0.409%
		Pr_{owc}	0.0152 Pa	0.531 %	0.029 % (calib.) 1.500% (sens.)	1.591 %
	H=0.025 m T=1.64 s	η_{inc}	0.0271 m	1.422 %	0.130 % (calib.) 0.100 % (sens.)	1.431 %
		T_{inc}	1.636 s	0.185 %	-	0.185 %
		η_{owc}		0.898 %	0.167 % (calib.) 0.100 % (sens.)	0.919 %
		Pr_{owc}	0.0221 Pa	0.452 %	0.029 % (calib.) 1.500% (sens.)	1.567 %
	H=0.025 m T=2.19 s	η_{inc}	0.0267 m	1.052 %	0.130 % (calib.) 0.100 % (sens.)	1.065 %
		T_{inc}	2.1770 s	0.323 %	-	0.323 %
		η_{owc}		0.468 %	0.167 % (calib.) 0.100 % (sens.)	0.507 %
		Pr_{owc}	0.0260 Pa	0.997 %	0.029 % (calib.) 1.500% (sens.)	1.801 %
Irregular waves	Hs=0.025 m; Tp=1.72 s	$P_{irr,inc}$	-	0.368 %	-	0.368 %
	Hs=0.042 m; Tp=1.72 s	$P_{irr,inc}$	-	0.387 %	-	0.387 %
	Hs=0.058 m; Tp=1.72 s	$P_{irr,inc}$	-	0.422 %	-	0.422 %
	All irregular waves	Pr_{owc}	-	-	0.029 % (calib.) 1.500% (sens.)	1.8 %
All waves		Z	2.0 %			
		d	1.0 m $\pm$ 0.01 m			
		g	9.807 m/s^2 $\pm$ 0.0057 m/s^2			
		ρ_w	998.8 kg/m^3 $\pm$ 1 kg/m^3			

346 ### 5.1.3 Combined uncertainty evaluation

347 Following [19], the Monte Carlo method is implemented to calculate the combined uncertainty of the
348 Capture Width Ratio (CWR), which is given by

$$CWR = \frac{P_{owc}}{P_{inc}D}, \qquad (7)$$

where P_{owc} is the mean power generated by the OWC, P_{owc} is the incident wave power and *D* is the width of the device. The incident wave power for regular waves is calculated from

$$P_{reg.inc} = \frac{1}{2}\rho_w g \left(\frac{H}{2}\right)^2 c_g, \qquad (8)$$

in which ρ_w is the water density, *g* is acceleration due to gravity, *H* is the wave height, and c_g is the group velocity. For the waves under consideration, the formula for c_g in transitional water is used, given by

$$c_g = \frac{c}{2}\left[1 + \frac{2kd}{\sinh 2kd}\right], \quad (9)$$

where $c = \omega/k$ is the wave celerity, *k* is the wave number determined by iterative solution of the dispersion relation $\omega^2 = gk \tanh kd$, in which ω is the angular frequency given by $\omega = 2\pi/T_{inc}$, T_{inc} being the incident wave period.

The formula for incident wave power for irregular waves for a given spectrum is

$$P_{irr,inc} = \frac{1}{2}\rho_w g^2 \int_0^\infty C_h(\omega) S(\omega) \frac{d\omega}{\omega}, \quad (10)$$

where $\mathrm{S}(\omega)$ is the power spectral density (obtained using a fast Fourier transform of the water surface elevation time series), and $\mathrm{C_h}(\omega)$ is a modification factor for wave power in finite water depth given by

$$C_h = \frac{k_0}{k}\left[1 + \frac{2kd}{sinh\, 2kd}\right], \qquad (11)$$

in which k_0 is the wave number in deep water.

The instantaneous power generated by the OWC is calculated from

$$P_{inst}(t) = Pr_{owc}(t)\, Q, \qquad (12)$$

where $Pr_{owc}(t)$ is the instantaneous pressure in the OWC chamber measured by the pressure sensors and Q is the flow or air volume flux through the orifice. *Q* is determined by solving

$$Q = \overline{v_c} A_c, \qquad (13)$$

where A_c is the area of the free surface inside the chamber, $\overline{v_c}$ is a 5-point moving average of the instantaneous velocity v_c of the free surface as it moves up and down within the OWC chamber. In this research, v_c is calculated by dividing the change in water level (i.e. the wave probe data from inside the OWC) over a single time step by the time between readings.

Q may also be determined from

$$Q = C_d A_o \sqrt{\frac{2|\Delta Pr|}{\rho_a}}, \qquad (14)$$

in which C_d is the orifice coefficient, A_o is the area of the orifice, ΔPr is the change in pressure in the OWC at each timestep, and ρ_a is the air density. Using Equation 14 necessitates determining C_d experimentally, which involves obtaining the flowrate in the water column (proportional to the velocity of column flow, i.e. the differential of the OWC's wave probe reading) and the differential of the chamber pressure reading using the manual or mechanical methods described in Section 2.2. In

any experimental system, differentiation results in signal noise and the experimental determination of C_d involves two signals requiring differentiation. Furthermore, the pressure reading in particular is subject to high frequency fluctuations. A moving average is applied to the pressure signal (time domain filtering) in order to get a cleaner signal prior to differentiation, however, like all filter operations this will reduce the magnitude of the signal as well as shift the signal response slightly. Additionally, since both experimental pressure and flowrate values are fluctuating, the discharge coefficient C_d, which is proportional to the division of these two fluctuating signals, will constantly vary. Equation 14 applies a single averaged value of C_d, and therefore any results obtained using this equation will have a high degree of uncertainty. Therefore, in this research, *Q* is calculated using Equation 13.

The mean power is then determined by integrating the instantaneous power over the analysis period:

$$P_{owc} = \frac{1}{T_{analysis}} \int_0^{T_{analysis}} Pr_{owc} Q \, dt. \qquad (15)$$

The above formulae allow us to determine what uncertainty values must be propagated in order to get an overall uncertainty for the CWR. Breaking down the CWR formula, the uncertain quantities associated with each element are shown in Table 4.

Table 4 List of uncertain quantities in CWR formula

	Uncertain quantities
Power: regular waves	$U_{P_{owc}} = f(U_{\eta_{owc}}, U_{Pr}, U_Z)$ $U_{P_{reg,inc}} = f(\, U_T, U_g, U_{\rho_w}, U_{\eta_{inc}}, U_d)$
Power: irregular waves	$U_{P_{owc}} = f(U_{\eta_{owc}}, U_{Pr}, U_Z)$ $U_{P_{irr,inc}} = f(\, U_{A-P_{inc}}, U_g, U_{\rho_w}, U_d)$
CWR	$U_{CWR} = f(U_{P_{owc}}, U_{P_{inc}})$

For each of the quantities listed in Table 4, a normal distribution is generated (in Matlab) characterised by the mean (μ) and the standard deviation (σ), where μ is the measured (e.g. *H*) or known (e.g. *g*, ρ_w) value, and σ is the standard uncertainty previously presented in Table 3. For example, the incident wave power for regular waves is calculated according to Equation 8, in which the values of in which ρ_w, *g*, and *H* are sampled from normal distributions. The group velocity, c_g, is calculated using randomly sampled values of *g*, the water depth *d*, and the period *T*. A similar method is applied to calculate the power generated by the irregular waves, and the power generated by the OWC. In order to account for uncertainties due to factors such as air compressibility, U_Z, that do not form part of the calculations, a normal distribution is created with μ = 0 mean and σ = u_s. This distribution is then randomly sampled and added to the relevant power calculation (e.g. P_{OWC}). The CWR is then calculated using Equation 7.

This process is repeated within each MC iteration to produce *N* values of the CWR where *N* is the number of MC iterations. The combined uncertainty, u_c, of the CWR is then determined by calculating the standard deviation of the *N* MC iterations. The results are presented in Table 5.

5.1.4 Expanded uncertainty evaluation

The expanded uncertainty is calculated by applying a coverage factor, *k*, to the combined uncertainty obtained from the MC method. The coverage factor can be obtained from a *t*-distribution table and its value is dependent on the number of samples (see for example [23]). The GUM [17] recommends a simplified approach for choosing *k* in measurement situations characterised by probability distributions that are approximately normal and where there is a significant number of samples. Here, the number of samples is the number of MC iterations (*N* = 10,000). Therefore, for a 95% confidence level the GUM recommends assuming a value of *k* = 2 to obtain the expanded uncertainty. The results are presented in Table 5, Figure 6 and Figure 7. The highest uncertainty is associated with regular waves where *T* = 1.64 s. This is primarily due to the higher Type A uncertainties associated with the wave probe measurements (see Table 3). In the case of the wave probe measurement inside the water column, this increased uncertainty is likely due to more energetic free surface motions within the chamber around the resonance period. The histograms provide a useful way to visualize the output of the MC method by clearly showing the spread in the results. Included on the histograms are red, yellow and purple lines indicating the mean, lower and upper bounds respectively of the 95% confidence interval.

In general, the uncertainties associated with the basin tests are relatively low compared with other similar experimental research [7]. This is primarily due to the method of calculating the OWC power, which avoided use of the orifice calibration coefficient and instead determined the power using the internal wave probe and pressure sensor data. The irregular wave expanded uncertainties were observed to be slightly lower than the regular waves

Table 5 Combined and expanded uncertainties

Ref	Wave details	Mean CWR	$u_{c,CWR}$ (*N*=1,000)	U_{CWR} (95% C.I.)
RW_A	H=0.025 m; T = 1.28 s	0.245	+/- 2.21 %	+/- 4.41 %
RW_B	H=0.025 m; T = 1.64 s	0.260	+/- 3.55 %	+/- 7.09 %
RW_C	H=0.025 m; T = 2.19 s	0.280	+/- 2.93 %	+/- 5.86 %
IW_A	Hs = 0.025 m; Tp = 1.72 s	0.267	+/- 2.04 %	+/- 4.08 %
IW_B	Hs = 0.042 m; Tp = 1.72 s	0.215	+/- 2.06 %	+/- 4.12 %
IW_C	Hs = 0.058 m; Tp = 1.72 s	0.188	+/- 2.06 %	+/- 4.11 %

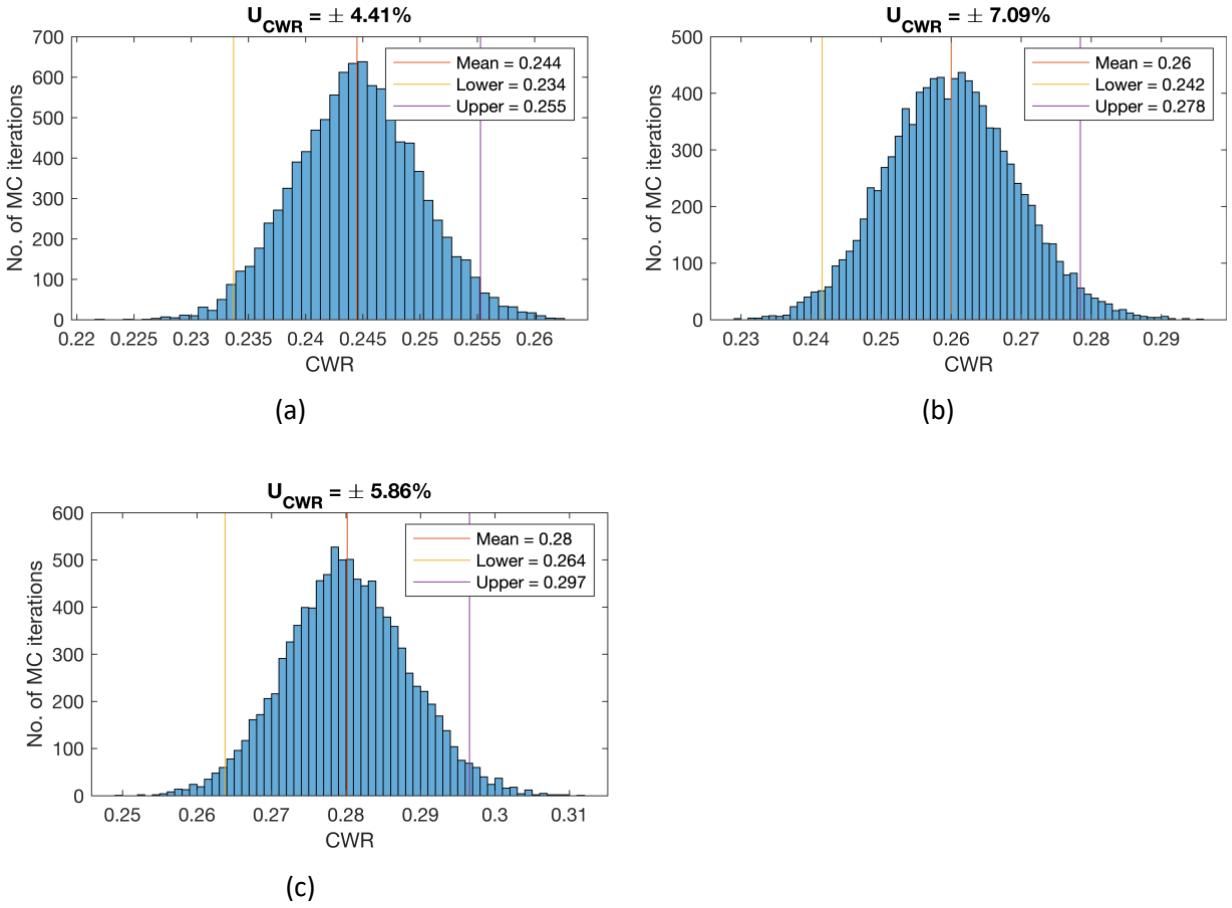

436 *Figure 6 Histogram of CWR values and associated expanded uncertainty, U_{CWR}, for (a) H = 0.025 and T = 1.28 s; (b) H =*
437 *0.025 m and T = 1.64 s; and (c) H = 0.025 m and T=2.19 s*

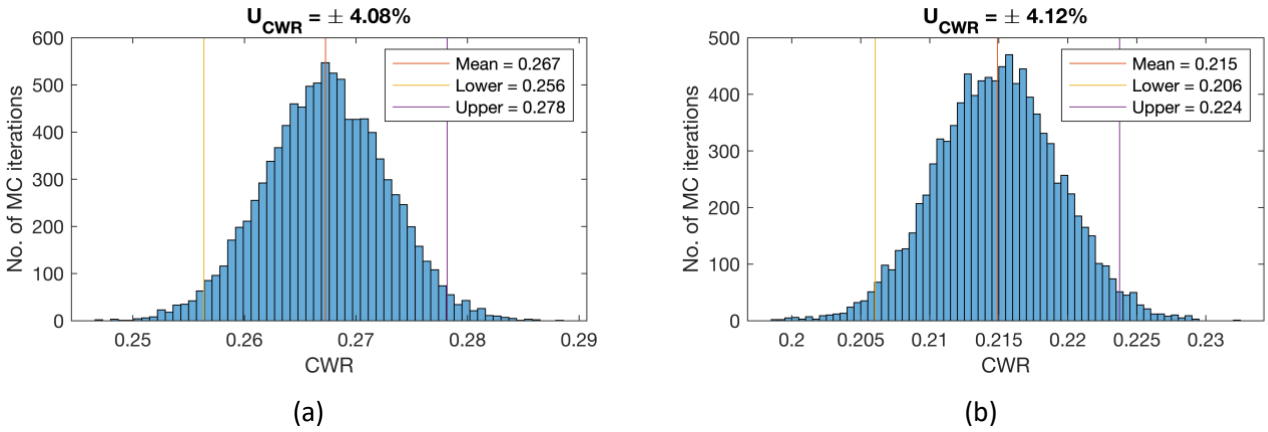

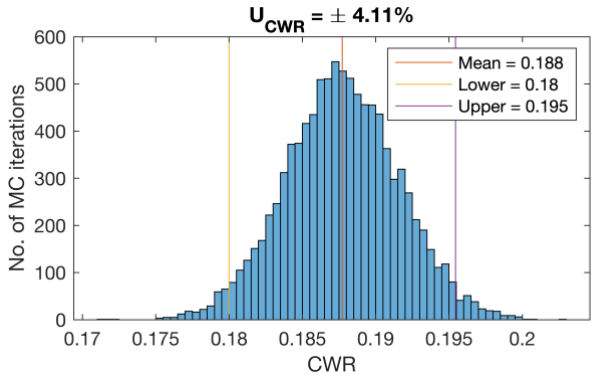

Figure 7 Histogram of CWR values and associated expanded uncertainty U_{CWR} for (a) Hs = 0.025 m and Tp = 1.72 s; (b) Hs = 0.042 m and Tp =1.72 s; and (c) Hs = 0.058 m and Tp = 1.72 s

5.1.5 Sensitivity analysis of selected standard uncertainties

The standard uncertainty associated with the parameter *Z* in Table 3 was based on engineering experience, and a sensitivity study was carried out to demonstrate the impact that a range of values would have on the expanded uncertainty of the CWR, U_{CWR}. Values of $u_{s,Z}$ ranging from 0.5 % to 10% were considered and the results for wave condition RW_B (*H* = 0.025 m, *T* = 1.64 s) are presented in Table 6 below. As $u_{s,Z}$ is added on to the uncertainty associated with the OWC power calculation, it has a linear impact on the overall uncertainty of the CWR. In contrast, the standard uncertainty of the pressure measured in the OWC chamber, while of a similar order of magnitude, does not have a significant impact on the overall expanded uncertainty (see Table 6). This is because the uncertainty associated with the pressure measurement relates to the instantaneous pressure in the chamber whereas the figure for OWC power (P_{owc}) that feeds into the CWR formula (Equation 6) is an average value. Therefore the uncertainty associated with the measurements within the chamber are 'averaged out'. Similar results were observed by applying a range of 0.5% to 10% to $u_{s,\eta\,owc}$, i.e. the standard uncertainty of the water level measurements inside the OWC chamber.

Table 6 Sensitivity analysis results for different values of standard uncertainties for Z and pressure measurement (base case indicated in bold)

U_{CWR} (%) RW_B		Standard uncertainty of *Z*, $u_{s,Z}$					
		0	0.5 %	1.0 %	**2.0 %**	5.0 %	10.0 %
Standard uncertainty of Pr_owc, $u_{s,Pr\,owc}$	0.5 %	5.74	5.84	6.10	7.05	11.46	21.16
	1.0 %	5.74	5.93	6.14	7.02	11.66	21.04
	1.567 %	5.74	5.86	6.09	**7.09**	11.58	20.95
	2.0 %	5.75	5.91	6.12	7.07	11.54	20.90
	5.0 %	5.84	5.86	6.13	7.10	11.62	20.82
	10.0 %	5.83	5.97	6.21	7.17	11.62	20.71
	20.0 %	6.31	6.32	6.55	7.51	11.83	20.89

In contrast, varying the standard uncertainty associated with the incident wave height measurements has a very significant impact on the accuracy of the CWR as illustrated in Table 7. For $u_{s,Z}$ = 2 %, varying $u_{s\eta\_inc}$ from 0.5% to 10 % results in UCWR increasing from 4.56 % to 42.59 %. The Type A uncertainty accounts for most of this standard uncertainty; this underscores the importance of calibrating the incident wave field to ensure consistent and repeatable conditions.

Table 7 Sensitivity analysis for a range of values of standard uncertainties for Z and incident wave height (base case indicated in bold)

U_{CWR} (%) RW_B		Standard uncertainty of Z, $u_{s,Z}$					
		0 %	0.5 %	1.0 %	**2.0 %**	5.0 %	10.0 %
Standard uncertainty of η_{inc}, $u_{s\eta\_inc}$	0.5 %	2.11	2.37	2.89	4.56	10.31	19.99
	1.0 %	4.09	4.21	4.57	5.65	10.80	20.30
	1.431 %	5.78	5.83	6.10	**7.09**	11.70	20.89
	2.0 %	7.92	8.05	8.27	9.00	12.73	21.69
	5.0 %	20.28	20.40	20.26	20.87	22.64	28.74
	10.0 %	42.68	42.46	41.94	42.59	43.58	46.68

6 Influence of reflections

Reflections during wave tank testing are inevitable, even with mitigating measures such as passive beaches and active absorption in place. Therefore, reflections must be quantified to establish the degree to which they influence the experimental results. This can be done through manual application of the Funke - Mansard method described in [15] although the wave generation software typically used in test facilities often has built-in functionality to perform these calculations giving a reflection coefficient, K_r, and a breakdown of the combined, incident and reflected time-series. The wave generation software in the Ocean Basin where the present model was tested implements the six-probe Funke and Mansard reflection analysis method [15]. The global positions of the six wave probes set up normal to the direction of wave propagation (see WP1-6 in Figure 2) are fed into the software which then the processes wave calibration data to give a reflection coefficient each regular wave under consideration as well as the incident, reflected and combined time-series. The reflection coefficient results are presented in Table 8 and indicate that reflections are more significant for lower frequency waves.

Table 8 Calculated reflection coefficients for regular wave conditions

Ref	Regular Wave Conditions	Average K_r for 5 repeats in Ocean Basin
RW_A	T = 1.28s, H = 0.025m	0.188
RW_B	T = 1.64s, H = 0.025m	0.307
RW_C	T = 2.19s, H = 0.025m	0.341

In order to determine the impact of reflections in this study, three different datasets for three regular wave conditions (RW_A: H = 25mm, T = 1.28s ; RW_B: H = 25mm, T = 1.64s; and RW_C: H = 25mm T = 2.19s) were examined. The first dataset of regular waves not impacted by reflections as described in Section 5.1.1 (Dataset 1), i.e. it consists of a short ~15 s time series before the waves reflected by the beach reached the model location. Dataset 2 is the combined (incident and reflected) wave field for the full test run after wave ramp up (~90 s); and Dataset 3 is the incident wave field only, obtained from the reflection analysis. For each of these datasets, the average wave height, H, was calculated, as well as the associated Type A uncertainty. Using the average wave heights, the incident wave power was calculated using Equation 8, and the results are summarised in Table 9. The values for Type A uncertainty are a function of the wave heights measured at the model location, and the number of waves in the time series. The highest error is associated with Dataset 1, but this is due to the lower number of samples compared with the other two datasets. Given the large number of samples in Datasets 1 and 2, the relatively large Type A error observed for the combined wave field indicates the variability in the wave heights at the model location due to reflections.

The Dataset 2 results for RW_A show that reflections caused constructive interference at the model location, resulting in a larger mean wave height, H, and incident wave power P_{inc} than was observed for the other two datasets. Dataset 1 and 3 are in good agreement, indicating that the reflection analysis was successful. Values are presented in Table 9 for the power produced by the OWC (P_{OWC}) and the CWR for each dataset. It is not possible to assess the impact of reflections on the device itself, as it was not feasible to distinguish the changes in water level in the OWC column caused by the incident and reflected waves. Therefore, the CWR was calculated using the power generated by the OWC without accounting for reflections (i.e. the power generated from the waves that struck the model during testing). Thus, only the CWR for Dataset 1 is not influenced by reflections and can be assumed to represent the true value (plus or minus the expanded uncertainty calculated in the previous section). Therefore, compared with Dataset 1, the calculated CWR for both Datasets 2 and 3 significantly underestimate the CWR for wave condition RW_A. For wave condition RW_C, the opposite phenomenon is observed: significant destructive interference at the model location results in a large underestimation of incident wave power and as a result, a hugely overestimated value of the CWR associated with Dataset 2. While the results for wave condition RW_B are more comparable across the three datasets, the impact of the reflections is observed in both the incident wave power for Dataset 2, and also the OWC power in Datasets 2 and 3. This indicates that the water column is influenced to a relatively significant degree by the reflected wave field.

It is likely that different results would be obtained with the model in a different location in the basin, depending on whether constructive or destructive interference is predominant at that point and highlights the importance of knowing both the incident and combined wave height at the measurement point. This study underlines the importance of accounting for reflections, either by running short tests to avoid contamination by reflections, or by conducting a reflection analysis. Long duration tests with the model in the basin and tests with irregular waves will still be contaminated by reflections, however. Numerical wave basins could be very useful in this regard as they can allow a user to specify open boundaries and thus run long duration simulations with no reflections; or be configured to represent the wave basin in question, and be used to calculate reflections at any point in the basin. Significant research has gone into the development of numerical wave basins [24–28], much of which is focused on simulating the interaction of waves with structures and has produced high fidelity but computationally intensive models. Simplified bespoke models designed for individual test facilities could be used to good effect to support offshore renewable energy tank testing campaigns in terms of determining optimal model placement within the wave basin. As computational costs reduce, validated higher fidelity models can be utilised in place of long duration tank tests in order to determine WEC performance.

527 *Table 9 Reflection analysis of selected regular waves*

		Dataset 1 (Short time series, no reflections)	**Dataset 2** (Full time series, combined wave field)	**Dataset 3** (Full time series, incident wave field only)
RW_A	Mean *H* (m)	0.0247	0.0280	0.0247
H = 0.025 m T = 1.28 s	$u_{A-\eta_{inc}}$ (%)	0.443	0.338	0.061
	P_{inc} (W/m)	0.782	1.072	0.835
	P_{OWC} (W)	0.0574	0.0482	0.0482
	CWR	0.245	0.150	0.193
RW_B	Mean *H* (m)	0.0271	0.0280	0.0269
H = 0.025 m T = 1.64 s	$u_{A-\eta_{inc}}$ (%)	1.422	0.287	0.029
	P_{inc} (W/m)	1.333	1.429	1.340
	P_{OWC} (W)	0.104	0.110	0.110
	CWR	0.260	0.256	0.273
RW_C	Mean *H* (m)	0.0267	0.0207	0.029
H = 0.025 m T = 2.19 s	$u_{A-\eta_{inc}}$ (%)	1.052	0.120	0.024
	P_{inc} (W/m)	1.768	1.074	2.113
	P_{OWC} (W)	0.149	0.151	0.151
	CWR	0.280	0.468	0.238

528 # 7 Conclusion

529 This paper provides a methodology for undertaking uncertainty analysis to quantify measurement
530 uncertainty in a wave basin setting for an OWC WEC. This relatively simple device was chosen to
531 minimise the sources of uncertainty. Repeat tests, calibration data and engineering experience
532 provided values for Type A and B uncertainties from which the standard uncertainty for each
533 parameter of interest was determined. Uncertainty was propagated using the Monte Carlo method in
534 order to determine the uncertainty associated with the capture width ratio of the device which was
535 found to be in the region of 4-7% for regular waves and 4% for irregular waves at a 95% confidence
536 level. The results indicate that the test was carried out with a reasonably high level of accuracy within
537 the parameters of the experiment. A sensitivity analysis revealed that the accuracy of the incident
538 wave field measurements had the most significant bearing on the expanded uncertainty of the CWR.
539 It is important to note that these results do not quantify the uncertainty due to scale effects (see
540 Section 2.2), and that the power performance results of an OWC at this scale may not be a reliable
541 indicator of the expected power performance of a full scale prototype (refer to [8] for a more detailed
542 study and discussion of scale effects in relation to a fixed OWC).

An additional analysis of reflections in the basin indicated that reflections have a significant impact and care should be taken to account for reflections to avoid misleading experimental results. Ideally, reflections in the whole basin would be characterised in advance by means of extensive physical measurements or by utilising calibrated numerical models.

Although guidance exists on how uncertainty should be evaluated when carrying out physical tank testing, such analysis is not generally carried out in a typical tank testing campaign. Similarly, guidance exists on how to assess the impact of reflections on model performance, but such analyses are not typically carried out during a commercial testing campaign. In general, standardised procedures for tank testing have not been widely adopted and test facilities tend to follow their own in-house procedures. EU supported research projects such as MaRINET2 will establish guidelines for both laboratory and field testing, from which standard procedures can ultimately be developed. It is important that uncertainty analysis forms an integral part of any such procedures as well as guidance on determining reflections so that individual device developers and the research community as a whole can work towards reducing the uncertainties associated with testing and increase investor confidence in the sector.

8 Acknowledgements

This research received funding from the European Union Horizon 2020 Framework Programme (H2020) under grant agreement no 731084 of the Marine Renewables Infrastructure Network for emerging Energy Technologies (MaRINET2) project.

9 References

[1] European Commission. Technology readiness levels (TRL). Eur Comm 2014. https://ec.europa.eu/research/participants/data/ref/h2020/other/wp/2016_2017/annexes/h2020-wp1617-annex-g-trl_en.pdf (accessed November 2, 2020).

[2] Qiu W, Sales Junior J, Lee D, Lie H, Magarovskii V, Mikami T, et al. Uncertainties related to predictions of loads and responses for ocean and offshore structures. Ocean Eng 2014;86:58–67. https://doi.org/10.1016/j.oceaneng.2014.02.031.

[3] Robertson AN, Bachynski EE, Gueydon S, Wendt F, Schünemann P, Jonkman J. Assessment of Experimental Uncertainty for a Floating Wind Semisubmersible Under Hydrodynamic Loading. Vol. 10 Ocean Renew. Energy, ASME; 2018, p. V010T09A076. https://doi.org/10.1115/OMAE2018-77703.

[4] ASME. Test Uncertainty, Preformance Test Codes. 2013.

[5] Desmond CJ, Hinrichs J-C, Murphy J. Uncertainty in the Physical Testing of Floating Wind Energy Platforms' Accuracy versus Precision. Energies 2019;12:435. https://doi.org/10.3390/en12030435.

[6] McCombes T, Johnstone C, Holmes B, Myers LE, Kofoed JP. EquiMar D3.4 Best practice for tank testing of small marine energy devices. 2010.

[7] Nader J-R, Penesis I, Orphin J, Howe D. Experimental Uncertainty Analysis of an OWC Wave Energy Converter. 2017.

[8] Orphin J. Uncertainty in Hydrodynamic Model Test Experiments of Wave Energy Converters. University of Tasmania, 2020. https://doi.org/10.13140/RG.2.2.12979.66088.

[9] Newman J. Marine Hydrodynamics. The MIT Press; 1977.

[10] Schmitt P, Elsäßer B. The application of Froude scaling to model tests of Oscillating Wave Surge Converters. Ocean Eng 2017;141:108–15.

[11] Benreguig P, Vicente M, Dunne A, Murphy J. Modelling Approaches of a Closed-Circuit OWC Wave Energy Converter. J Mar Sci Eng 2019;7:23. https://doi.org/10.3390/jmse7020023.

[12] Howe D, Nader J-R, Macfarlane G. Experimental Analysis into the Effects of Air Compressibility in OWC Model Testing. 2018.

[13] Sheng W, Thiebaut F, Babuchon M, Brooks J, Lewis A, Alcorn R. Investigation to air compressibility of oscillating water column wave energy converters. Int. Conf. Offshore Mech. Arct. Eng., vol. 55423, American Society of Mechanical Engineers; 2013, p. V008T09A005.

[14] Dimakopoulos AS, Cooker MJ, Bruce T. The influence of scale on the air flow and pressure in the modelling of Oscillating Water Column Wave Energy Converters. Int J Mar Energy 2017;19:272–91. https://doi.org/https://doi.org/10.1016/j.ijome.2017.08.004.

[15] Mansard EPD, Funke ER. The Measurement of Incident and Reflected Spectra Using a Least Squares Method. Coast. Eng. 1980, New York, NY: American Society of Civil Engineers; 1980, p. 154–72. https://doi.org/10.1061/9780872622647.008.

[16] Goda Y, Suzuki Y. Estimation of incident and reflected waves in random wave experiments. 15th Coast. Eng. Conf., 1976, p. 828–45.

[17] BIPM, IEC, IFCC, ILAC, ISO, IUPAC, et al. JCGM 100:2008: Evaluation of measurement data - Guide to the expression of uncertainty in measurement. 2008.

[18] ITTC. Uncertainty Analysis for a Wave Energy Converter. 2017.

[19] Orphin J, Penesis I, Nader J-R. Uncertainty Analysis for a Wave Energy Converter: the Monte Carlo Method. n.d.

[20] Judge F, McAuliffe FD, Sperstad IB, Chester R, Flannery B, Lynch K, et al. A lifecycle financial analysis model for offshore wind farms. Renew Sustain Energy Rev 2019;103:370–83. https://doi.org/10.1016/j.rser.2018.12.045.

[21] Müller K, Cheng PW. Application of a Monte Carlo procedure for probabilistic fatigue design of floating offshore wind turbines. Wind Energ Sci 2018;3:149–62. https://doi.org/10.5194/wes-3-149-2018.

[22] ITTC-Recommended Procedures Fresh Water and Seawater Properties ITTC Quality System Manual Recommended Procedures and Guidelines Procedure Fresh Water and Seawater Properties. 2016.

[23] T-Distribution Table (One Tail and Two-Tails) - Statistics How To n.d. https://www.statisticshowto.com/tables/t-distribution-table/ (accessed December 16, 2020).

[24] Judge FM, Orszaghova J, Taylor PH, Borthwick AGL. A 2DH hybrid Boussinesq-NSWE solver for near-shore hydrodynamics. Coast Eng 2018;142. https://doi.org/10.1016/j.coastaleng.2018.08.014.

[25] Judge FM, Hunt-Raby AC, Orszaghova J, Taylor PH, Borthwick AGL. Multi-directional focused wave group interactions with a plane beach. Coast Eng 2019. https://doi.org/10.1016/j.coastaleng.2019.103531.

[26] Chow AD, Rogers BD, Lind SJ, Stansby PK. Numerical wave basin using incompressible smoothed particle hydrodynamics (ISPH) on a single GPU with vertical cylinder test cases. Comput Fluids 2019;179:543–62. https://doi.org/10.1016/j.compfluid.2018.11.022.

626 [27] Wen H, Ren B, Dong P, Wang Y. A SPH numerical wave basin for modeling wave-structure
627 interactions. Appl Ocean Res 2016;59:366–77. https://doi.org/10.1016/j.apor.2016.06.012.

628 [28] Hu ZZ, Greaves D, Raby A. Numerical wave tank study of extreme waves and wave-structure
629 interaction using OpenFoam®. Ocean Eng 2016;126.
630 https://doi.org/10.1016/j.oceaneng.2016.09.017.

631